

# Diurnal Land–Sea Rainfall Peak Migration over Sumatera Island, Indonesian Maritime Continent, Observed by TRMM Satellite and Intensive Rawinsonde Soundings

SHUICHI MORI, HAMADA JUN-ICHI, YUDI IMAN TAUHID, AND MANABU D. YAMANAKA\*

*Frontier Observational Research System for Global Change, Yokohama, Japan*

NORIKO OKAMOTO, FUMIE MURATA, AND NAMIKO SAKURAI

*Graduate School of Science and Technology, Kobe University, Kobe, Japan*

HIROYUKI HASHIGUCHI

*Radio Science Center for Space and Atmosphere (RASC), Kyoto University, Kyoto, Japan*

TIEN SRIBIMAWATI

*Agency for the Assessment and Application of Technology (BPPT), Jakarta, Indonesia*

(Manuscript received 27 June 2003, in final form 17 February 2004)

## ABSTRACT

The diurnal cycle of rainfall and its regional variation over Sumatera Island, Indonesian Maritime Continent, are examined using Tropical Rainfall Measuring Mission (TRMM) satellite precipitation radar (PR) and intensive rawinsonde sounding data. The TRMM PR sensor can detect raindrops directly, regardless of ground and cloud conditions, and can distinguish between convective and stratiform types of rainfall. Rainfall variation over this area was found to have the following characteristics: 1) convective rainfall with a broad peak between 1500 and 2000 LT predominates over the land region of Sumatera Island, whereas rainfall in the early morning, composed almost equally of stratiform and convective types, is predominant over the surrounding sea region. 2) A rainfall peak in the daytime and one in the nighttime migrate with time starting from the southwestern coastline of the island into the inland and offshore regions, respectively. The distance of each rainfall peak migration from the coastline is up to 400 km, and the average speed of migration is approximately  $10 \text{ m s}^{-1}$ . 3) Using intensive rawinsonde sounding data, it was also found that remarkable diurnal variations of wind, humidity, and stability appear in the lower troposphere corresponding to the migrating rainfall peaks over both the inland and the coastal sea regions.

The mechanism of the diurnal land–sea rainfall peak migration is discussed comprehensively using TRMM PR, intensive rawinsonde soundings, Geostationary Meteorological Satellite (GMS) data, objective reanalysis, and ground-based observation data. Finally, a crucial difference in rainfall peak migrating mechanisms is suggested between those toward the inland region in the daytime and the offshore region in the nighttime.

## 1. Introduction

The diurnal cycle of rainfall and its regional variations are important in the Tropics, where the synoptic-scale cyclones that cause rainfall in extratropical regions do not exist. Because tropical rainfall involves the uptake and release of significant amounts of latent heat of vaporization, understanding of the diurnal rainfall cycle

is also important in the study of large-scale energy and water cycles such as the Asian monsoon system. Previous studies using in situ rain gauge networks, limited rawinsonde observations, geostationary satellites [e.g., Geostationary Meteorological Satellite (GMS), Geostationary Operational Environmental Satellite (GOES), and Meteosat] infrared (IR) sensor, and atmospheric reanalysis data have gradually revealed that these variations have prominent interactions with local topographical features, as well as being dependent on complicated interactions among various scales of convective systems (e.g., Johnson and Kriete 1982; Janowiak et al. 1994; Nitta and Sekine 1994; Oki and Musiake 1994; Asai et al. 1998; Harada et al. 1998; Ohsawa et al. 2001). Most studies have indicated that diurnal rainfall variations in

\* Additional affiliation: Graduate School of Science and Technology, Kobe University, Kobe, Japan.

Corresponding author address: Shuichi Mori, Frontier Observational Research System for Global Change, 3173-25, Showamachi, Kanazawa-ku, Yokohama, Kanagawa 236-0001, Japan.  
E-mail: morishu@jamstec.go.jp

the Tropics have their peaks in the late evening over land regions and in the early morning over adjacent sea regions (e.g., Gray and Jacobson 1977; Murakami 1983; Houze et al. 1981).

Furthermore, remarkable regional changes in the phase of diurnal convective variations have been found by Nitta and Sekine (1994) and Ohsawa et al. (2001) in several regions in the Asian monsoon area, for example, the northeastern part of the Indochina Peninsula, the Andaman Sea, the northwestern coast of Kalimantan (Borneo) Island, and the southwestern coast of Sumatera Island, Indonesian Maritime Continent. Yang and Slingo (2001) also found a similar pattern of coherent diurnal convective variations propagating to offshore regions off the coastlines of the Indonesian islands, the Bay of Bengal, southwestward away from the Mexican coast, and off the West African coast, using the IR-sensor-based Cloud Archive User Service (CLAUS) global dataset. They explained the phase propagation away from the coastlines in several ways. For instance, an interaction between the orography and local land–sea-breeze circulation, gravity waves generated by developed convections, cold gravity currents generated under the developed convection, and an advection conveyed by the background wind flow were documented as candidates for its driving source. However, these results are based on only the IR-sensed cloud-top data, and their analysis has not integrated other data, for example, rain gauge network, radar, and rawinsonde soundings. Satomura (2000) and Okumura et al. (2003) examined the phase propagation of the rainfall diurnal cycle over the inland region of the Indochina Peninsula using the Regional Atmospheric Modeling System (RAMS) numerical model simulation and Thailand Meteorological Department (TMD) operational radar data, respectively, and found it was caused by eastward-traveling squall lines in the evening, which was consistent with the results of GMS IR channel 1 (IR1) sensor observations. Mapes et al. (2003a,b) and Warner et al. (2003), using the GOES precipitation index (GPI) dataset and the fifth-generation Pennsylvania State University–National Center for Atmospheric Research (PSU–NCAR) Mesoscale Model (MM5) numerical model simulation, also showed that a similar phase propagation of the diurnal rainfall cycle away from the coast of northwestern South America was caused by gravity waves originating from convection that developed along the coastline. However, no study has been done on the similar phenomena over Indonesian island regions.

On the other hand, it is also well known that the peak time of the variations observed by geostationary satellites' IR sensor shows a delay of approximately 3–4 h compared with those observed by ground-based radar and/or in situ rain gauge data (Houze et al. 1981; Ohsawa et al. 2001; Kubota and Nitta 2001; etc.). Because the IR sensor does not detect rainfall itself but cloud-top temperature, it may often misinterpret a high anvil region expanded from developed cumulonimbus as a

heavy rainfall region. A number of studies regarding rainfall diurnal variation have been conducted recently using the precipitation radar (PR) equipped on the Tropical Rainfall Measuring Mission (TRMM) satellite launched in 1997 because it has the advantage of detecting raindrops directly from space, which allows us to reveal the rainfall diurnal variation accurately over the globe (e.g., Nesbitt and Zipser 2003; Sorooshian et al. 2002; Takayabu 2002). In addition, TRMM PR can distinguish rainfall characteristics using the 2A23 algorithm (Awaka et al. 1998) into three types of rainfall: stratiform, convective, and other. Since the former two types of rainfall have completely different latent heat profiles from each other (Houze 1982), it is also important to quantify these variations separately. Takayabu (2002) has shown the average features of diurnal variations of these two types of rainfall in both land and oceanic regions over the globe, revealing remarkable differences both between the rainfall types and between the regions. However, this has not clarified the diurnal variations of rainfall characteristics over complex regions including both coastal sea and mountainous topography such as the Indonesian Maritime Continent.

Since the Indonesian Maritime Continent is composed of many islands and the surrounding sea, both regional and temporal variations of rainfall may be quite complicated because of strong interactions between land and adjacent sea through their heterogeneous radiation properties and local circulations. In fact, a GCM simulation done by Neale and Slingo (2003) showed a serious systematic dry bias in this region using the Met Office Unified Model (UM) and had difficulty describing the diurnal rainfall variation. They suggested that this systematic error was caused by diurnally forced land–sea breezes and gravity waves generated by mesoscale convective complexes (MCCs) in this region. Moreover, the GCM simulations of the global circulation pattern showed that a significant role was played by the diurnal rainfall cycle in this region.

Seasonal and interannual variability over the Indonesian Maritime Continent including Sumatera Island have been examined by Hamada et al. (2002) using long-term statistical data. Diurnal variation of precipitating cloud was examined by Renggono et al. (2001) using a boundary layer radar (BLR) system at the Kototabang [0.20°S, 100.32°E; 865 m above mean sea level (MSL)] World Meteorological Organization (WMO) Global Atmosphere Watch (GAW) station in Sumatera Island. Murata et al. (2002) also documented a relation between rainfall amount at Kototabang and background wind circulation for a limited period. Moreover, a diurnal variation of precipitable water and its relation with local circulation for a limited period. Moreover, a diurnal variation of precipitable water and its relations with local circulation over Kototabang was examined by Wu et al. (2003) using the global positioning system (GPS). These studies have described unique characteristics of both regional and temporal rainfall and/or convection distri-

butions over this area, but the phase change (or propagation) feature of the diurnal cycle has not been addressed.

This study presents the characteristics of the diurnal rainfall cycle and its regional differences over the Indonesian Maritime Continent, especially around Sumatera Island, using the TRMM PR 3G68 product. Intensive rawinsonde sounding data at Kototabang and the Tabin (0.88°S, 100.35°E; 3 m above MSL) Indonesian Meteorological and Geophysical Agency (BMG) station are also utilized to examine background atmospheric conditions relevant to the diurnal rainfall variation. In section 2, the data used in this study, which are TRMM PR, intensive rawinsonde soundings, GMS, objective reanalysis, outgoing longwave radiation (OLR), and surface measurement data observed in collaboration with the BMG and the Indonesian Agency for the Assessment and Application of Technology (BPPT), are described. In section 3, striking features of diurnal land–sea rainfall peak migration away from the southwestern coastline of Sumatera Island, which advances toward the inland region in the daytime and the offshore region in the nighttime, and the interaction with lower-tropospheric circulations are documented. In section 4, unique rainfall characteristics over the coastal sea region and a possible mechanism of the rainfall peak migration are discussed. Section 5 is the conclusion of this study.

## 2. Observations and data

### a. TRMM satellite data

The TRMM satellite was launched in November 1997 and has successfully provided rainfall data up to the present time. We utilized the TRMM 3G68 product distributed by the TRMM Science Data and Information System (TSDIS) office as well as the standard products—for example, 2A12, 2A23, 2A25, and 3A25—distributed by the National Aeronautics and Space Administration (NASA) Goddard Distributed Active Archive Center (DAAC). The 3G68 product contains an hourly gridded ASCII format dataset reporting TRMM instruments, for example, the PR and TRMM Microwave Imager (TMI), which estimate near-surface rain rate. It includes 24 h of hourly grids in a single daily file, with horizontal resolution of  $0.5^\circ \times 0.5^\circ$ . The dataset contains three kinds of statistical rain rate based on the standard products 2A25 (PR), 2A12 (TMI), and 2B31 (PR and TMI combined) and supplies the convective rain-rate fraction for each rain rate.

We made a composite dataset of near-surface rain rate based only on the PR sensor for 3 yr (1998–2000) and calculated the hourly rain rate for convective, other (stratiform), and total rainfalls for each grid element. Each hourly grid rainfall data were smoothed over a 4-h running mean to minimize the sampling errors ( $\pm \sigma/\sqrt{n}$ ) of the rainfall diurnal cycle following the analysis of Negri et al. (2002), where  $\sigma$  is the standard deviation

of data and  $n$  is the total sampling data number used for smoothing. The sampling errors in this study are 13% (offshore region) to 17% (land region) on average (see error bars in Fig. 2) and show good results, comparable to those of Negri et al. (2002).

Generally, a passive microwave sensor has difficulty in resolving rainfall rate over the land area because the microwave emissivity over the land is essentially higher than that over the ocean and is inhomogeneous in both area and time (e.g., Rodgers and Siddalingaiah 1983; Grody 1984; Heymsfield and Fulton 1992). Furthermore, since TMI data involve a systematic error over coastline areas in which both land and ocean regions are included in a pixel (mixcel problem), we decided to analyze only PR sensor data over the Indonesian Maritime Continent area, since it is composed of a lot of islands and surrounding sea.

A number of reports on the mesoscale convective system (MCS) have been published (e.g., Houze and Betts 1981; Steiner et al. 1995; Rickenbach and Rutledge 1998; Mohr et al. 1999; Nesbitt and Zipser 2003) that include the squall line systems composed of developed convective and stratiform clouds that are generally responsible for heavy rainfall in the wet Tropics, for example, the western Pacific, Atlantic Ocean, Amazon, and the Maritime Continent. Because convective and stratiform rainfalls have completely different latent heat release profiles, as Houze (1982) showed, they may interact with large-scale environments in a different way. A number of studies have shown the distribution and ratio of convective and stratiform rainfalls over various regions using different techniques (e.g., Houze 1977; Williams et al. 1995; Steiner et al. 1995). However, Williams et al. (1995) demonstrated that the ratio varied greatly depending on the particular classification techniques and threshold values of brightband definition used. Therefore, it is important that the TRMM PR provides information on rain-type classification globally and solely by using a single algorithm (2A23).

### b. Intensive rawinsonde sounding data

In Indonesia, operational rawinsonde observations are currently conducted by the BMG once every two days at 10 observatories including the Tabin station, and once daily at the Jakarta Airport. All the soundings are launched at 0000 UTC (0700 LT); thus diurnal variations of upper wind and other atmospheric parameters cannot be resolved. Furthermore, the Kototabang GAW station is not assigned as an operational rawinsonde sounding observatory. Detailed information of the operational rawinsonde observation and data processing systems in Indonesia were described by Okamoto et al. (2003).

We used intensive rawinsonde sounding data obtained during 1–28 November 2001 at Kototabang and 12–18 November 2001 at Tabin. This was one of our intensive observation periods (IOPs), which began in March 2001

and corresponds to the main rainy season in west Sumatra. Vaisala RS-15GH (GPS) and Meisei RS3-89A rawinsondes were employed for the intensive observations at Kototabang and Tabing, respectively. We made observations four times a day (0000, 0600, 1200, 1800 UTC) and took soundings at four other times (0300, 0900, 1500, and 2100 UTC) at Kototabang during 8–21 November 2001. Both rawinsonde sounding systems provide vertical profiles of pressure, temperature, humidity, and horizontal wind with a height resolution of approximately 10 m.

### c. Surface data

Most BMG stations measure daily or 3-hourly rainfall using the BMG standard manual accumulation rain gauge, and hourly rainfall data cannot be archived as a standard routine. Therefore, we installed tipping-bucket rain gauges (equipped with Vaisala automatic weather stations MAWS201), as well as surface pressure, temperature, humidity, and solar radiation sensors at both the stations. Minimum sensitivity for rainfall amount and the temporal resolution of recorded data are 0.2 mm and 1 min at Kototabang (Vaisala QMR101 precipitation sensor) and 0.5 mm and 10 min at Tabing (Ogasawara RS-102). These observations have continued since August 1999 at Kototabang and November 2001 at Tabing. However, because of a malfunction with the MAWS201 installed at Tabing, no rainfall data were recorded during the enhanced sounding period (12–18 November 2001). Hence, 3-hourly accumulated rainfall data observed by the BMG standard manual rain gauge at Tabing were used in this study.

### d. GMS cloud data

Blackbody brightness temperature ( $T_{BB}$ ) data observed by the GMS IR1 sensor ( $11.5 \mu\text{m}$ ) were used during November 2001 in this study, as provided by the Japan Meteorological Agency (JMA) through Kochi University, Japan. Spatial and temporal resolution of the  $T_{BB}$  data are  $0.05^\circ \times 0.05^\circ$  and 1 h, respectively. They are suitable to trace the change of a developing cloud area in a short time though they have the disadvantage that only the cloud-top height can be detected.

### e. Other data

Objective reanalysis data averaged in November 2001, provided by the National Centers for Environmental Prediction (NCEP)–NCAR office, were used to analyze a large-scale ( $\sim 1000$  km) diurnal variability. Spatial and temporal resolution of the data are  $2.5^\circ \times 2.5^\circ$  and 6 h, respectively. There are approximately 90 pilot balloon observatories in Indonesia, and BMG carries out the sounding at least three times (0700, 1300, and 1600 LT) a day. All the sounding data at each observatory are sent to WMO Global Telecommunications

System (GTS), and NCEP–NCAR reanalysis uses these GTS exchange data for initialization as well as 3-hourly surface land synoptic data, satellite-observed humidity, and upper wind data, etc. (Kalnay et al. 1996; Kistler et al. 2001). Hence, this dataset cannot resolve a diurnal variability of mesoscale phenomena because of its coarse resolution but can supply useful information of that in a large-scale ( $\sim 1000$  km) domain.

OLR datasets with spatial and temporal resolutions of  $2.5^\circ \times 2.5^\circ$  and pentad (5-days mean), respectively, distributed by the National Oceanic and Atmospheric Administration (NOAA) Climate Prediction Center (CPC) were also used in this study.

## 3. Results

### a. Diurnal variations of rainfall amount and type over Sumatra Island

The Indonesian Maritime Continent is one of the regions with the largest amount of rainfall anywhere on the globe (Ramage 1968). Sumatra Island in particular receives the most rainfall along the southwestern coastal region as shown in Fig. 1a, since it faces the Indian Ocean and directly receives moist air with the southwesterly monsoon. Sumatra Island measures approximately 1500 km by 400 km, or roughly the same dimension as Honshu, the main island of Japan. Sumatra Island has a significant mountain range along its southwestern coastline with an average height of 2000 m and a maximum of 3805 m (Mt. Kerinci). Figure 1b shows the regional variation of the annual mean difference of rainfall during 0000–1100 LT (hereafter referred to as morning rain) from that during 1200–2300 LT (hereafter referred to as evening rain) observed by TRMM PR. It shows more rainfall in the evening than in the morning over the land regions of relatively large islands, for example, Sumatra, Jawa, and Kalimantan, but more rainfall in the morning than in the evening over the coastal sea regions surrounding the islands. The southwestern coastline of Sumatra Island, the Strait of Malacca, and surrounding coastline of Kalimantan especially show a strong contrast between the evening rain over land regions and the morning rain over coastal sea regions. The amplitude of these contrasts decreases with the distance from each coastline.

We study the interesting contrast of rainfall characteristics between Sumatra Island and the nearby southwestern coastal sea area by examining the regional variability of the diurnal rainfall cycle. Diurnal variations of rainfall over the Kototabang GAW station averaged for an area of  $1.5^\circ \times 1.5^\circ$  (region 1 in Fig. 1a) over the southwestern coastal sea region (region 2 in Fig. 1a) and over the offshore region (region 3 in Fig. 1a) of Sumatra Island are shown in Fig. 2.

Region 1 (Fig. 2a) shows a clear bimodal variation with both a main peak in the evening and a subpeak in the middle of the night. The main peak of convective



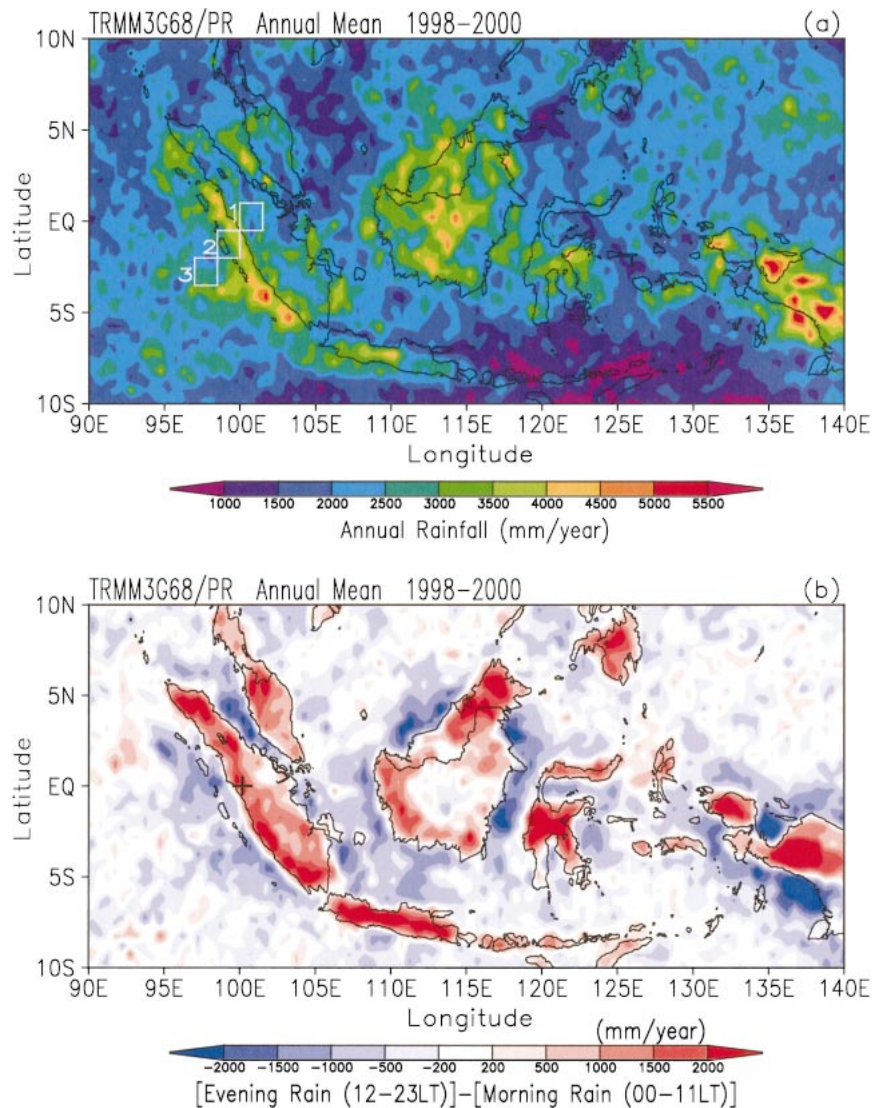


FIG. 1. (a) Annual mean rainfall over the Indonesian Maritime Continent observed by TRMM PR during 1998–2000. Small rectangles around Sumatera Island indicate the following regions: 1) region 1 (land region), 2) region 2 (coastal sea region), and 3) region 3 (offshore region). Horizontal scale of each region is  $1.5^{\circ} \times 1.5^{\circ}$ . The Kototabang GAW station ( $0.20^{\circ}\text{S}$ ,  $100.32^{\circ}\text{E}$ ; 865 m MSL) is located in region 1. (b) Regional variation of annual mean difference between morning rain (0000–1100 LT) and evening rain (1200–2300 LT) over the area observed by TRMM PR. Positive value indicates more rainfall observed from 1200 to 2300 LT than from 0000 to 1100 LT. The black cross (+) indicates the Kototabang GAW station.

rainfall appears at 1700 LT, whereas that of stratiform rainfall appears around 1800–2000 LT, though variations are minimal. More than 70% of the rainfall amount comes from evening rain for any rain types, and the convective rainfall fraction is 63% of the daily mean. Furthermore, the dominant rainfall type is completely different between evening and morning rains, that is, approximately 70% of evening rain is composed of convective rainfall, whereas roughly 50% of morning rain is stratiform. In region 2 (Fig. 2b), a main rainfall peak appears clearly after midnight, while a weaker peak also appears in the evening. Both stratiform and convective

rainfalls have their main peaks at almost the same time (0100–0200 LT), whereas a subpeak of stratiform rainfall in the evening (1900 LT) follows the convective one (1400 LT). In contrast to region 1, approximately 60% of the rainfall amount comes from morning rain for any rain types, and the convective rainfall fraction is 57% of the daily mean. Thus the contribution of stratiform rainfall is slightly higher than that in region 1. Furthermore, the diurnal variation in region 3 (Fig. 2c) has a quite different feature from that in the other two regions. The peak of total rainfall in region 3 is broad, weak, and shifted later in the morning (0900 LT) than

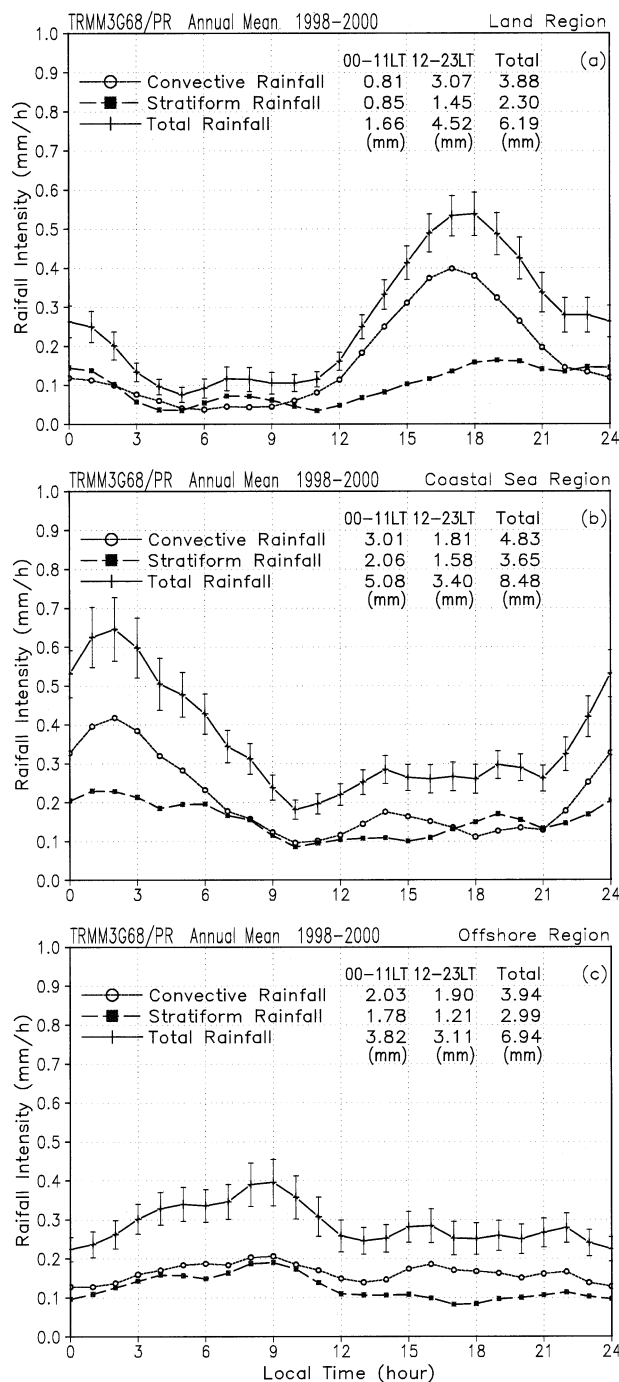


FIG. 2. Diurnal variations of rainfall rate averaged over  $1.5^\circ \times 1.5^\circ$  boxes as observed by TRMM PR. Annual mean average in (a) region 1 (land region), (b) region 2 (coastal sea region), and (c) region 3 (offshore region) in Fig. 1a, respectively. Solid line with open circle, dashed line with closed box, and solid line with cross indicate diurnal variations of convective, stratiform, and total rainfall rates, respectively. The sampling errors ( $\pm \sigma/\sqrt{n}$ ) are plotted as vertical bars with total rainfall rate lines. Small numbers shown in (a)–(c) are the daily amount of each rainfall fraction corresponding to the line (rainfall type) and column (LT).

in region 2. On the other hand, rainfall fraction in region 3 shows features similar to those in region 2, that is, approximately 60% of the rainfall amount comes from morning rain, and the convective rainfall fraction is 57% of the daily mean.

In earlier studies of the convective rainfall fraction, Takayabu (2002) found 50% over the ocean, and 61% over the land as a global average using TRMM PR, and Steiner et al. (1995) also found 52% at Darwin, Australia (coastal sea region), using a ground-based radar system. These are similar to the results of this study except for those over the ocean. This suggests that region 3 (offshore region) still has some characteristics of a coastal sea (i.e., having more convective rainfall fraction) compared with that of Takayabu's work. Indeed, Petersen and Rutledge (2001) defined the "coastal" as an ocean area within 500–1000 km of major landmasses, somewhat different from this work, and showed both radar reflectivity vertical structure histograms and lightning flash density data of "coastal" areas often resembled those of "continent" areas.

#### b. Rainfall peak migrations advancing from the coastline

The results in section 3a indicate that remarkable differences are found in the characteristics of diurnal rainfall variation over the land, coastal sea, and offshore regions. In this section, we examine the variation of the diurnal rainfall cycle at some distance from the southwestern coastline of Sumatera Island toward the land and the Indian Ocean.

Figure 3 shows a diurnal variation of rainfall horizontal distribution over Sumatera Island observed by TRMM PR averaged over 3 yr (1998–2000). Rainfall with its intensity above  $0.2 \text{ mm h}^{-1}$  is observed over the island after 1300 LT, then strong rainfall areas are concentrated along the southwestern coastline at 1600 LT. The rainfall area expands to inland regions and covers most of the island at 1900 LT, but other strong rainfall areas are generated over the coastal sea region along the southwestern coastline at 2200 LT. Rainfall over the coastal sea region expands its area into offshore regions during 0100–0700 LT, whereas rainfall areas over the island are almost cleared up during 0400–1000 LT.

A regional variation of the diurnal rainfall cycle observed by TRMM PR averaged in a domain perpendicular to the southwestern coastline of Sumatera Island (Fig. 4a) is shown as Fig. 5a. Arrows  $\alpha$  and  $\beta$  in Fig. 5a indicate the migrating directions of evening rain over the land region and morning rain over the coastal sea region, respectively. A rainfall peak migrates from the southwestern coastline toward an offshore region of the Indian Ocean during 0000–1200 LT (arrow indicated by  $\beta$ ). On the other hand, another peak migrates from the coastline toward the inland region of Sumatera Island during 1200–2400 LT (arrow indicated by  $\alpha$ ). Earlier studies presented differences of rainfall character-

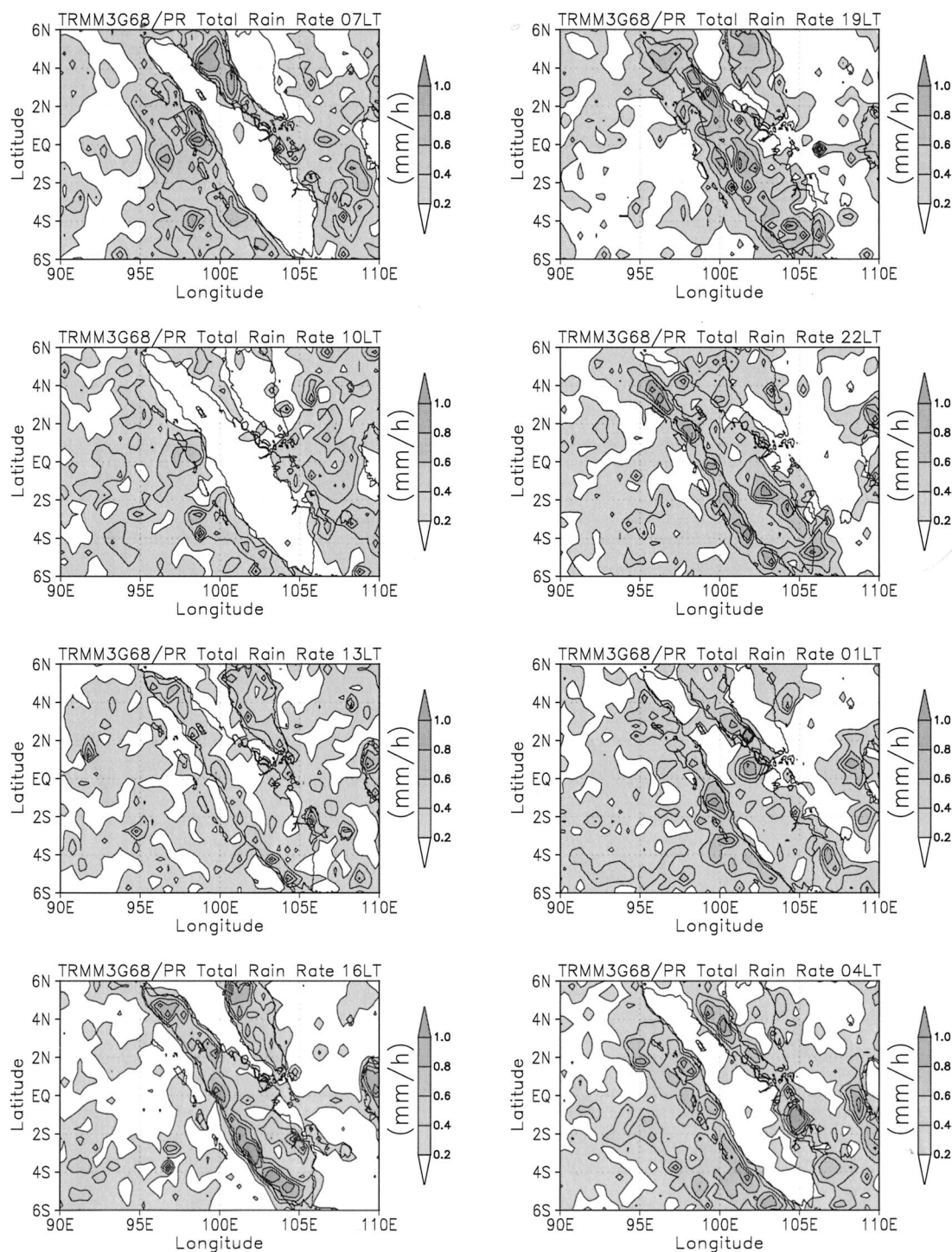


FIG. 3. Diurnal variation of rainfall horizontal distribution over Sumatra Island observed by TRMM PR averaged over 3 yr (1998–2000). Areas with rainfall intensity above  $0.2 \text{ mm h}^{-1}$  are shaded.

istics with respect to their diurnal variation over the land, coastal sea, and offshore regions using GMS IR1 data (e.g., Ohsawa et al. 2001; Kubota and Nitta 2001), but their results show some disagreement with those derived from ground-based in situ rain gauge data. Pos-

sible reasons for the disagreements are that, since the passive IR1 sensor detects the  $T_{\text{BB}}$  of cloud top, a high cold anvil cloud area spread out from cumulonimbus might be misunderstood as a rainfall area and that an upper-level cloud carried by wind might be regarded as

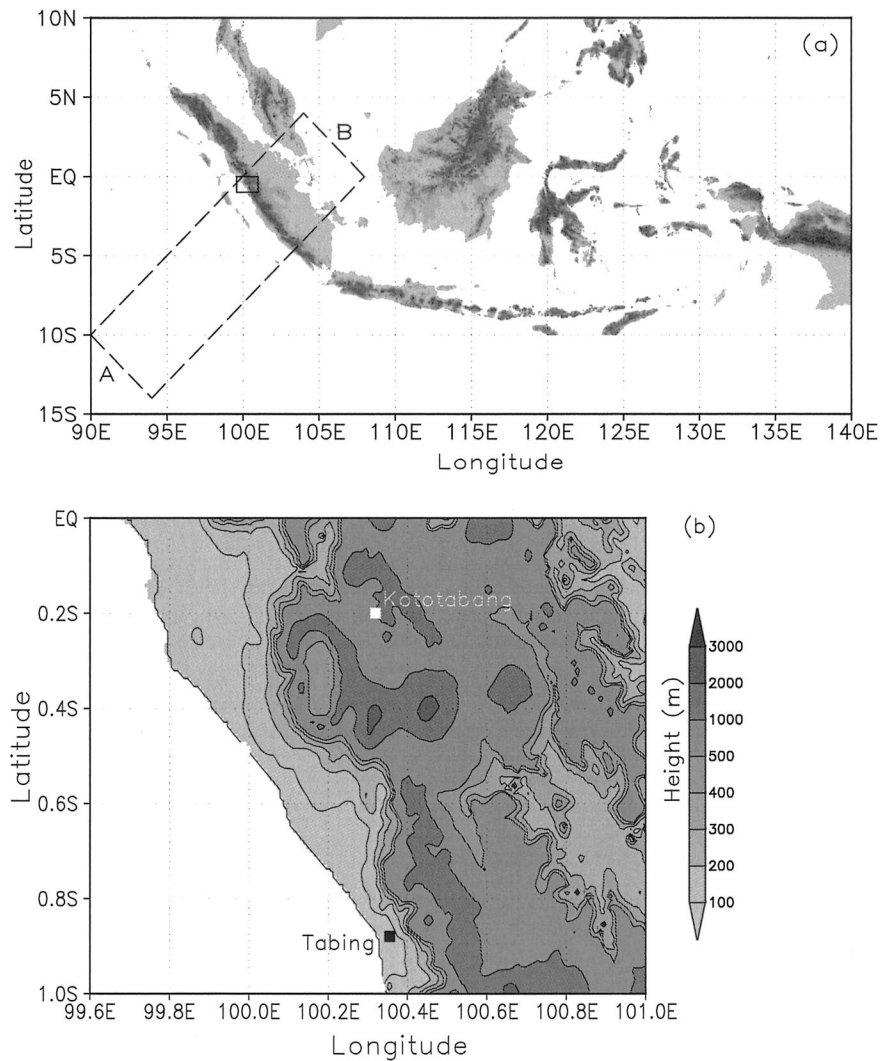


FIG. 4. (a) Topography of the Indonesian Maritime Continent. A large rectangle with dashed line around Sumatra Island (A–B) is a domain of calculation for rainfall regional variations shown in Fig. 5. Notations of locations A and B correspond to those in Fig. 5. (b) Topography of a small box with solid line over Sumatra Island shown in (a). Locations of Kototabang GAW station (0.20°S, 100.32°E; 865 m above MSL) and BMG Tabing station (0.88°S, 100.35°E; 3 m above MSL) are indicated by white and black boxes, respectively.

a migration of rainfall area on the ground. On the other hand, TRMM PR does not produce such errors since it is an active microwave sensor that detects raindrops directly. Thus Fig. 5a clearly shows migrating rainfall peaks. The rainfall peak  $\alpha$  travels 400 km (from 1600 km at 1500 LT  $\sim$  2000 km at 0600 LT), and  $\beta$  travels the same distance (from 1550 km at 2100 LT  $\sim$  1150 km at 0700 LT) when we follow the rainfall peak above 0.4 mm h<sup>-1</sup> of total rain rate in Fig. 5a. Hence, the average speed of migration is roughly 10 m s<sup>-1</sup> (those of peak  $\alpha$  and  $\beta$  are 7.4 and 11.1 m s<sup>-1</sup>, respectively). The migration speed of the rainfall peak  $\alpha$  is constant all the time, whereas that of  $\beta$  looks different between the area within about 200 km from the coastline (until 0600 LT) and the farther offshore area (after 0600 LT).

The main part of the rainfall peak  $\beta$ , which is shown until 0600 LT, appears to continue southwestward slowly even after 0600 LT within 200 km from the coastline. After 0600 LT, more rainfall seems to develop at large distances ( $\sim$ 300 km) southwest of the coastline.

The difference in rainfall characteristics between evening rain over the land region and morning rain over the coastal sea region is also examined. Figure 5b shows a distance–time variation of convective rainfall fraction over the same domain as that in Fig. 5a. The total rainfall intensity in each region is similar, as shown in Fig. 5a, but a remarkable difference in the convective rainfall fraction appears between evening rain over the land and morning rain over the coastal sea. Convective rainfall is predominant in the evening rain over the land, where-

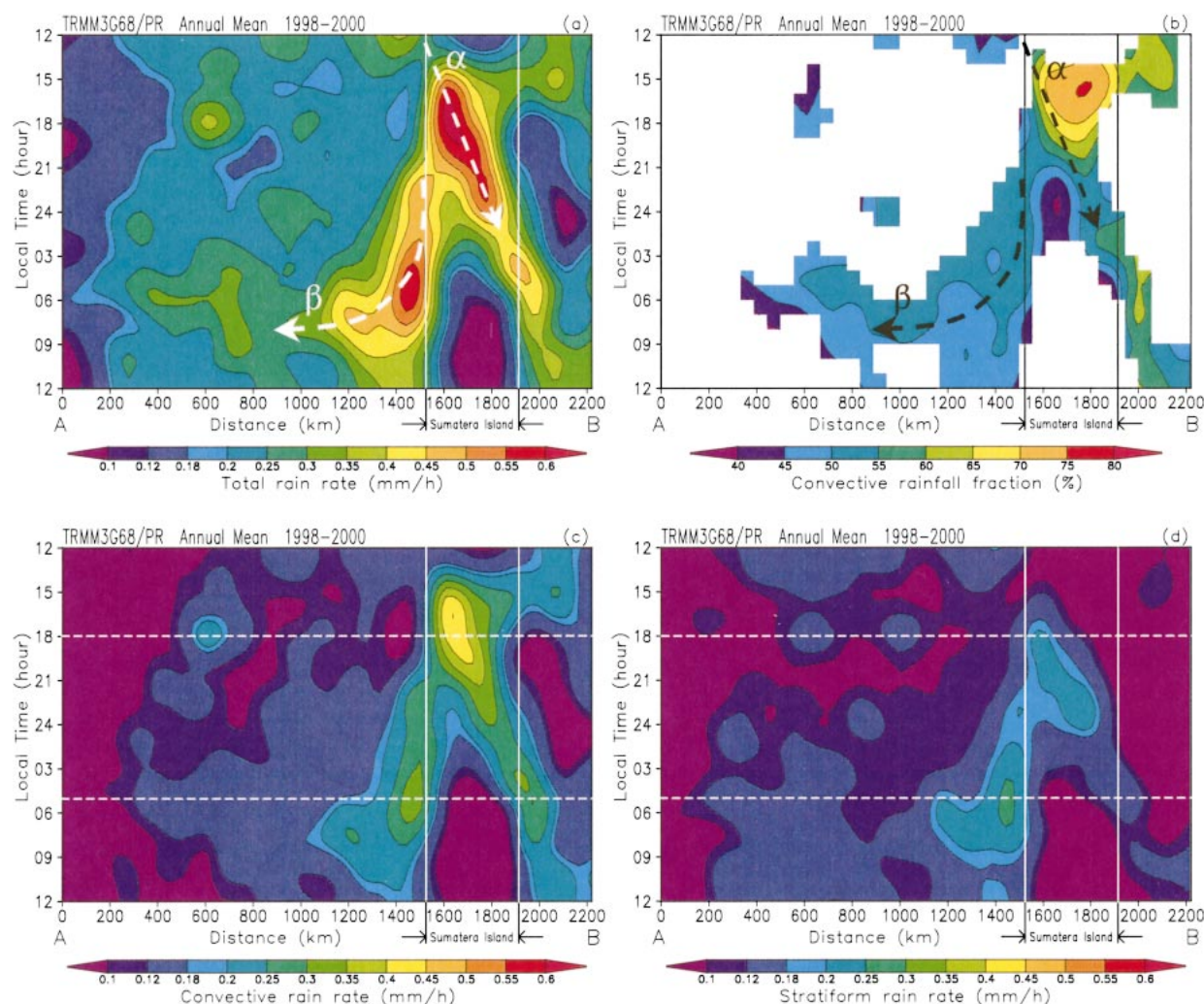


FIG. 5. Regional variation of the diurnal rainfall cycle over the rectangular area between A and B shown in Fig. 4a observed by TRMM PR. Vertical solid lines indicate coastlines of Sumatra Island. Variations of (a) total rain rate and (b) convective rainfall fraction. The area with total rainfall rate above  $0.25 \text{ mm h}^{-1}$  is shaded in (b). Arrows  $\alpha$  and  $\beta$  with dashed line indicate the migrating directions of evening rain over the inland region and morning rain over the coastal sea region, respectively. Variations of (c) convective and (d) stratiform rain rates. Upper and lower horizontal white dashed lines show local peak times of evening rain over the land and morning rain over the coastal sea, respectively.

as the morning rainfall over the coastal sea is composed almost equally of both stratiform and convective rainfalls. Furthermore, the convective rainfall fraction in the morning rain over the coastal sea does not vary significantly with time or distance from the coastline. Regional developments of convective and stratiform rainfalls are presented in Figs. 5c and 5d, respectively. The time of rainfall maximum in the evening over the land is coincident with that of the convective rainfall maximum, but that of the stratiform rainfall maximum is delayed approximately 3 h. On the other hand, the rainfall maximum in the early morning over the coastal sea region shows good agreement between convective and stratiform rainfalls.

Phase delays in the movement of rainfall peak time toward offshore regions from a coastline were also doc-

umented by Nitta and Sekine (1994) and Ohsawa et al. (2001) in some parts of southeast Asia using GMS IR1 data. Nitta and Sekine (1994) applied Fourier analysis to the convective index ( $I_C$ ) determined by the  $T_{BB}$  threshold, but Ohsawa et al. (2001) pointed out several problems with this analysis: 1) the phase of diurnal variation strongly depends on the threshold value of  $I_C$ , and 2) the first component of Fourier analysis does not necessarily show the actual peak time of convection. Hence, Ohsawa et al. (2001) utilized the  $T_{BB}$  difference between IR1 and water vapor (WV) channels ( $\Delta T_{BB}$ ) as an index of convective activity and did not apply Fourier analysis to the data. Their results showed an abrupt change of peak time over the inland and offshore regions of northwestern Sumatra Island, while we document sequential phase delay on both sides of the southwestern

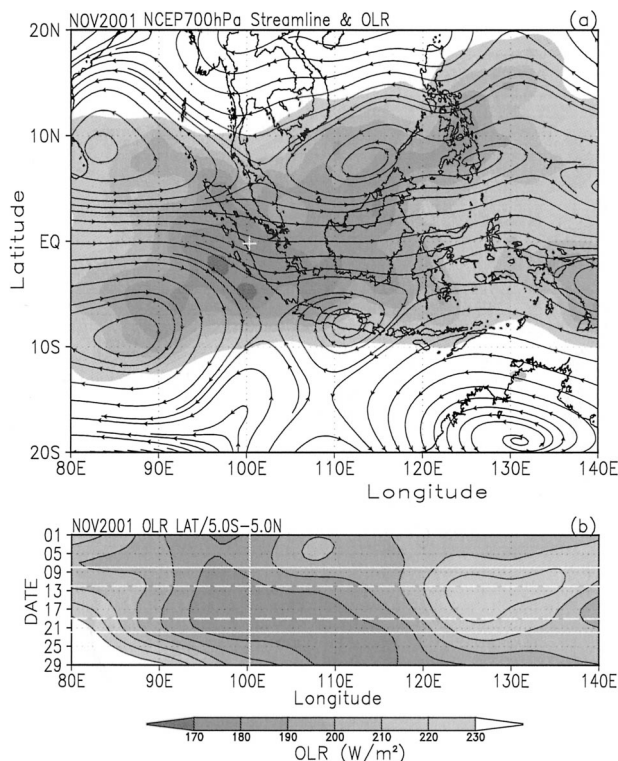


FIG. 6. (a) Composite streamline map at 700 hPa obtained from the NCEP–NCAR reanalysis dataset and OLR averaged over Nov 2001 and (b) time–lon cross section of OLR averaged over  $2.5^{\circ}S$ – $2.5^{\circ}N$  during Nov 2001. A white cross (+) in (a) shows the location of the Kototabang GAW station, and a vertical white line in (b) shows the lon of the station. Horizontal white solid and dashed lines in (b) show the duration of enhanced sounding periods at Kototabang (8–21 Nov) and Tabin (12–18 Nov), respectively.

coastline as shown in Fig. 5a. This suggests that the  $\Delta T_{BB}$  method still produces a systematic difference from the surface rainfall amount over Sumatera Island because Ohsawa et al. (2001) used only data for the period of the Asian summer monsoon in June–August (JJA), corresponding to the dry season over the central part of Sumatera Island (Hamada et al. 2002). Furthermore, they compared  $\Delta T_{BB}$  data with ground-based rain gauge data from four countries (Bangladesh, Thailand, Vietnam, and Malaysia) other than Indonesia, and the result might be expected to differ from our result with respect to the annual mean rainfall feature.

### c. Case study during IOP in November 2001

We examine lower-tropospheric structure and surface meteorological data as well as GMS IR1 data in this subsection to relate background conditions to diurnal rainfall peak migrations. Figures 6a and 6b show streamlines from the 700-hPa NCEP–NCAR reanalysis dataset and OLR averaged over November 2001 and a time–longitude cross section of OLR averaged over  $2.5^{\circ}S$ – $2.5^{\circ}N$  during the month, respectively. A white cross (+)

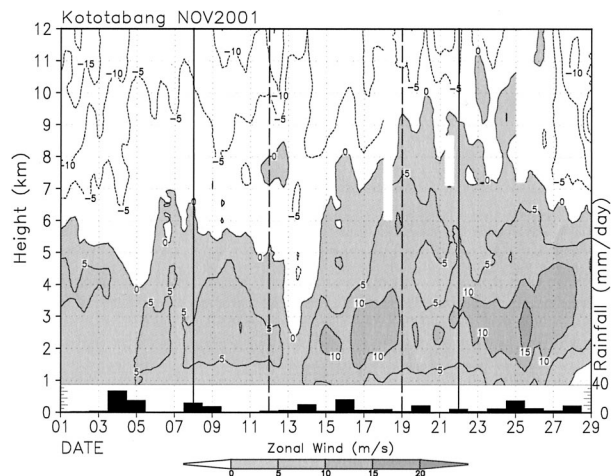


FIG. 7. Daily surface rainfall at Kototabang GAW station (bar graph) and time–height cross section of zonal wind contours observed by the intensive rawinsonde soundings in Nov 2001. Vertical black solid and dashed lines show the duration of enhanced sounding periods at Kototabang (8–21 Nov) and Tabin (12–18 Nov), respectively.

in Fig. 6a shows the location of Kototabang GAW station and a vertical white line in Fig. 6b shows the longitude of the station. Horizontal white solid and dashed lines in Fig. 6b show the duration of enhanced sounding periods at Kototabang (8–12 November) and Tabin (12–18 November), respectively. A low OLR region below  $200 W m^{-1}$  covers Sumatera Island, and westerly wind prevails over the island in this month. In addition, a large-scale disturbance passed Sumatera Island from west to east during this month. Figure 7 shows daily surface rainfall at the Kototabang GAW station (bar graph) and time–height cross section of zonal wind contours observed by the intensive rawinsonde soundings in November 2001. Vertical black solid and dashed lines show the duration of enhanced sounding periods at Kototabang (8–12 November) and Tabin (12–18 November), respectively. The total number of days with daily rainfall above 0.2 mm was 27, monthly rainfall was 185.6 mm, and maximum daily rainfall was 30.6 mm. The westerly wind was steady in the lower troposphere below approximately 7 km, whereas a steady easterly wind was observed above. The lower westerly wind increased and extended upward in the later part of the month corresponding to the eastward movement of a large-scale disturbance as shown in Fig. 6b.

Figures 8a and 8b show average diurnal variations of the tropospheric zonal wind component at the Kototabang GAW station and Tabin, respectively, as observed by intensive rawinsonde soundings. The topography and location of each station are shown in Fig. 4b. The peak time of westerly winds in the lower troposphere is approximately 2200 LT at Kototabang and 1900 LT at Tabin. These features suggest that the westerly winds centered at 2–3-km altitude advance from Tabin (sea side) to Kototabang (inland side) every evening, con-

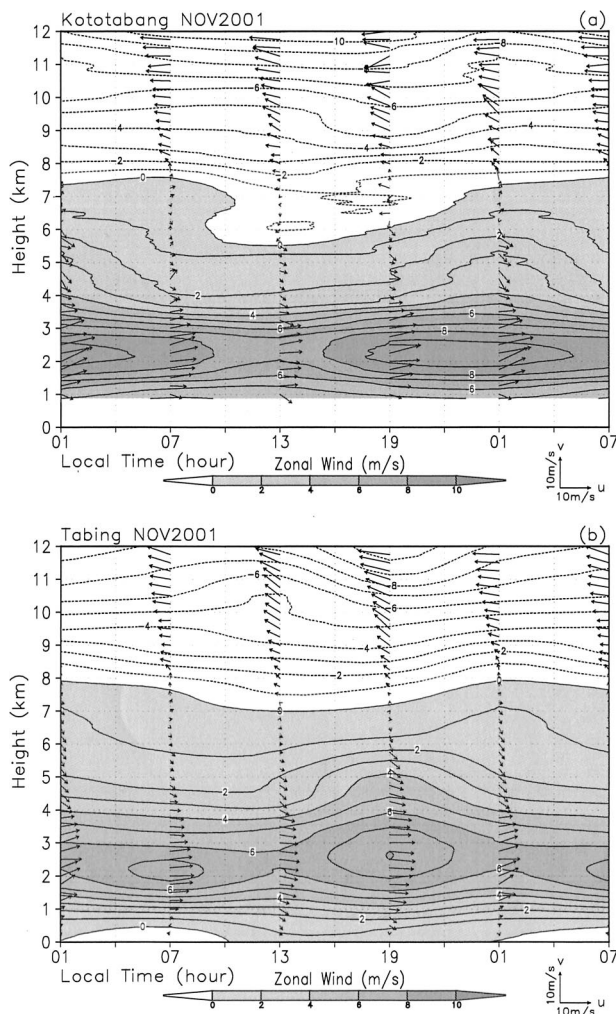


FIG. 8. Time-height cross sections of average diurnal variation of tropospheric zonal wind (contours) and horizontal wind vectors at (a) Kototabang GAW station and (b) Tabin observed by the intensive rawinsonde soundings in Nov 2001.

sistent with the migration of the rainfall peak as seen in Fig. 5a. Furthermore, a secondary westerly wind peak is shown at 0700 LT at Tabin and a counterflow (easterly wind) appears below 500 m almost simultaneously. Based on the topography around Tabin, as shown in Fig. 4b, this circulation seems to be a shallow land-breeze circulation that is independent of the westerly peak at 1900 LT.

Figure 9 shows diurnal variations of zonal and meridional wind anomalies at 2–3-km height (Figs. 9a,f), specific humidity anomaly below 3-km height (Figs. 9b,g), convective available potential energy (CAPE) and convective inhibition (CIN) (Figs. 9c,h), level of free convection (LFC) and lifting condensation level (LCL) (Figs. 9d,i), and surface rainfall (Figs. 9e,j) at Kototabang and Tabin. All the data were observed by the intensive rawinsonde soundings during 1–28 November at Kototabang and 12–18 November at Tabin in 2001.

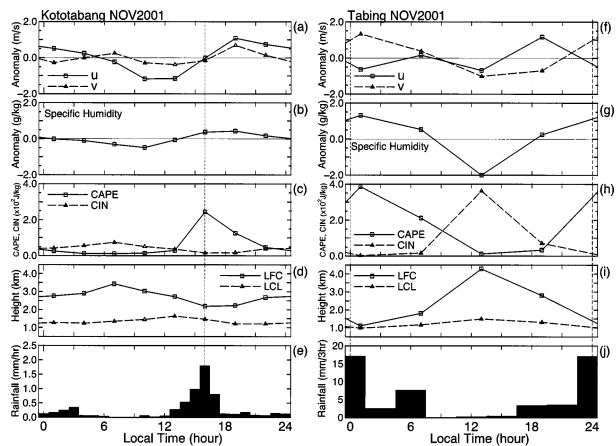


FIG. 9. (a),(f) Diurnal variations of zonal and meridional wind anomalies at 2–3 km; (b),(g) specific humidity anomaly below 3 km; (c),(h) CAPE and CIN; (d),(i) LFC and LCL; and (e),(j) surface rainfall at (left) Kototabang GAW station and (right) Tabin. All the data were observed by the intensive rawinsonde soundings during 1–28 Nov at Kototabang and 12–18 Nov at Tabin in 2001. Each anomaly is calculated as a deviation from the average value over the whole sounding period at the each station. Hourly rainfall data at Kototabang and 3-hourly accumulated rainfall data at Tabin were recorded by the Vaisala MAWS201 and the BMG standard manual rain gauge, respectively. Vertical dashed lines show the time of rainfall peak at the each station.

Because the 3-hourly (0400, 1000, 1600, and 2200 LT) soundings were carried out only during 12–21 November at Kototabang, we calculated 3-hourly data from each 6-hourly sounding dataset during 1–11 and 22–28 November by using a simple interpolation method. Then, the monthly mean data were obtained by averaging each 3-hourly dataset during 1–28 November. Each anomaly is calculated as a deviation from the average value over the whole sounding period at the each station.

Although these data were obtained within only 1 month, the surface rainfall at Kototabang is quite similar to that shown as the annual mean in TRMM satellite data for the inland region (region 1) shown in Fig. 2a. Specific humidity at Kototabang shows its minimum at 1000 LT and then increases until its broad maximum around 1600–1900 LT. CAPE also reaches its maximum at 1600 LT with a trend similar to that of rainfall. Then it decreases with time and the stratification becomes stable in the middle of the night through the next morning. A difference between LFC and LCL shows its minimum at 1600 LT coincident with the peak time of CAPE and rainfall amount. Zonal and meridional wind anomalies show their broad minimum at 1000–1300 LT and then tend to increase, reaching their maximum at 1900 LT. They are negative (easterly and northerly) approximately until the time of rainfall maximum (1600 LT) and then became positive (westerly and southerly).

In contrast, the variations at Tabin show completely different features from Kototabang. The location of the Tabin station is approximately 5 km inland from the coastline, but its rainfall characteristics are rather similar

to that of the coastal sea region (region 2) shown in Fig. 2b. Specific humidity and CAPE reach their maximum in the middle of the night (0100 LT), which is similar to the rainfall maximum time, and then tend to decrease until noon. A difference between LFC and LCL shows its minimum at 0100 LT, also coincident with the peak time of CAPE and rainfall amount. Petersen et al. (1996) also found similar diurnal variations of CAPE, rainfall, lightning flash, and cold-cloud area over the tropical western Pacific Ocean during the Tropical Ocean Global Atmosphere Coupled Ocean–Atmosphere Response Experiment (TOGA COARE). Lightning flash showed its peak at 0200 LT in the middle of the night, which was followed by the time of rainfall peak by 1 h, CAPE and cold-cloud area by 3 h. The zonal wind anomaly shows positive (westerly) just before the time of maximum rainfall (2300–0100 LT) and then becomes slightly negative (easterly) or zero until the early evening. In contrast, the meridional wind anomaly reaches its minimum (northerly) around the noon and its maximum (southerly) in the middle of the night (0100 LT), which is approximately coincident with the time of maximum rainfall. Based on Fig. 9, the maximum and minimum times of both specific humidity and CAPE are coincident with those of local rainfall amount. Zonal wind anomalies in the lower troposphere change their direction at the time of local peak rainfall from easterly to westerly at Kototabang, and from westerly to easterly at Tabing.

Sequential GMS IR1 data are utilized during this period in order to examine the movements of precipitating cloud systems. Figure 10 shows the diurnal variation of horizontal distribution of  $T_{BB}$  averaged over November 2001 around Sumatera Island. Similar to TRMM PR observed sequential rainfall distribution (Fig. 3), developing convective cloud tops higher than  $T_{BB} = 250$  K (approximately 8–9-km altitude) appear at 1600 LT over Sumatera Island along the southwestern coastline. The peak of cloud-top height first develops over the land and advances eastward with time during 1900–2200 LT, and then gradually disappears after expanding inland at 0100 LT. On the other hand, the high cloud-top area extends toward the coastal sea region during 2200–0100 LT, and then moves offshore. As mentioned in the previous subsection, high cloud area over coastal sea and offshore regions after 2200 LT is considered to be anvil cloud, generated by cumulonimbus that developed over inland regions and drifted westward. On the other hand, several cloud areas develop again inside of the broad expanded high cloud over the offshore region, which may not be just a drifted anvil cloud. They seem to involve a definite mechanism developing in the nighttime over the offshore regions, which are discussed in section 4. As mentioned in the previous sections, the GMS IR1 sensor, detecting only the cloud-top temperature, does not directly identify the region of strong rainfall, but the sequence of GMS IR1 imagery shown in Fig. 10 is roughly consistent with both the diurnal migration of the rainfall peak and the distribution of

convective rainfall fraction as shown in Figs. 5a and 5b, respectively.

Diurnal variations of horizontal wind anomaly and convergence fields at 200 and 700 hPa derived from the NCEP–NCAR reanalysis dataset averaged in November 2001 are shown in Figs. 11a and 11b, respectively, in order to examine the circulation on the scale of the entire island of Sumatera for comparison with the cloud system and rainfall peak migrations. Each anomaly is calculated as a deviation from the daily average value in this period. Figure 11b (700 hPa) shows clear convergence over Sumatera Island at 1300 LT, which then turns to weak divergence at 1900 LT. Finally, the divergence over the land region reaches its maximum at 0100 LT. In contrast, after the divergence reaches its maximum at 1300 LT over the surrounding ocean, the maximum convergence field takes over there at 1900 LT. The ocean is covered by a developed divergence field again, which is centered on the island, at 0100 LT, and only the areas with weak convergence are left in the northwestern and far southwestern sides of Sumatera Island. The diurnal cycle of the convergence field at 200 hPa (Fig. 11a) shows good counteragreement with that at 700 hPa. The sequence of the diurnal cycle in the convergence field is roughly consistent with the contrast of rainfall peak time distribution, that is, evening rain over the land and morning rain over the sea. However, the peak time of the convergence field appears 4–6 h earlier than that of rainfall over both the land and sea regions. Furthermore, it does not show the migration of rainfall peak and cloud system apparent in Figs. 3, 5, and 10 because of large spatial and temporal resolutions.

#### 4. Discussion

##### a. Difference of rainfall characteristics between land and coastal sea regions

In the previous sections, we have examined the differences of rainfall characteristics among the inland, coastal sea, and offshore regions of Sumatera Island both in nighttime and in daytime. A high stratiform rainfall ratio was observed over the inland region through the night and until early morning, and over both the coastal sea and offshore regions throughout the day. This result is roughly consistent with those of earlier studies, but most of these did not describe diurnal variations. Renggono et al. (2001) examined diurnal rainfall variations over Serpong (6.4°S, 106.7°E; 50 m above MSL) in west Jawa and Kototabang by classifying them into convective and stratiform rainfalls using a BLR. Our results are almost consistent with their results regarding the variation of convective rainfall over the inland region, but the amplitude of our stratiform rainfall variation seems to be weaker. The peak time delay between stratiform and convective rainfall is up to 3 h in their study, which is almost similar to our results in Figs. 2a, 5c and 5d (2–3-h delay).

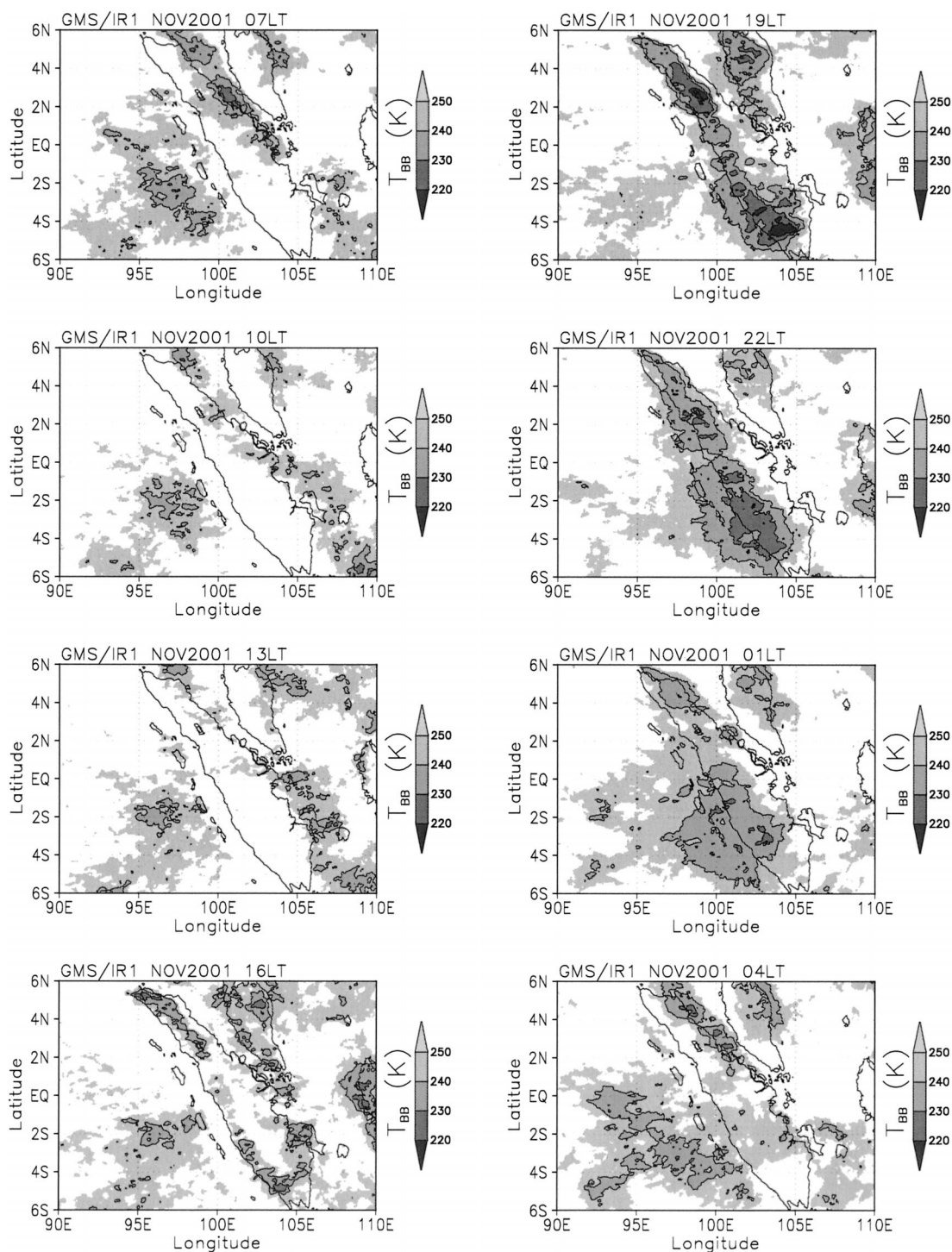


FIG. 10. Diurnal variation of horizontal distribution of GMS IR1 imagery averaged over Nov 2001. The shaded area corresponds to  $T_{BB}$  below 250 K. Cloud-top height of  $T_{BB} = 250$  K corresponds to approximately 8–9-km altitude based on the sounding data in this period.

The increase of convective rainfall compared with stratiform in the afternoon over the inland region (Fig. 2a) is remarkable, but both convective and stratiform rainfalls show similar variations in the nighttime over

the coastal sea region (Fig. 2b). This suggests that most of the precipitating clouds over the inland region in the afternoon are composed of isolated convective clouds accompanied by a smaller component of stratiform (an-

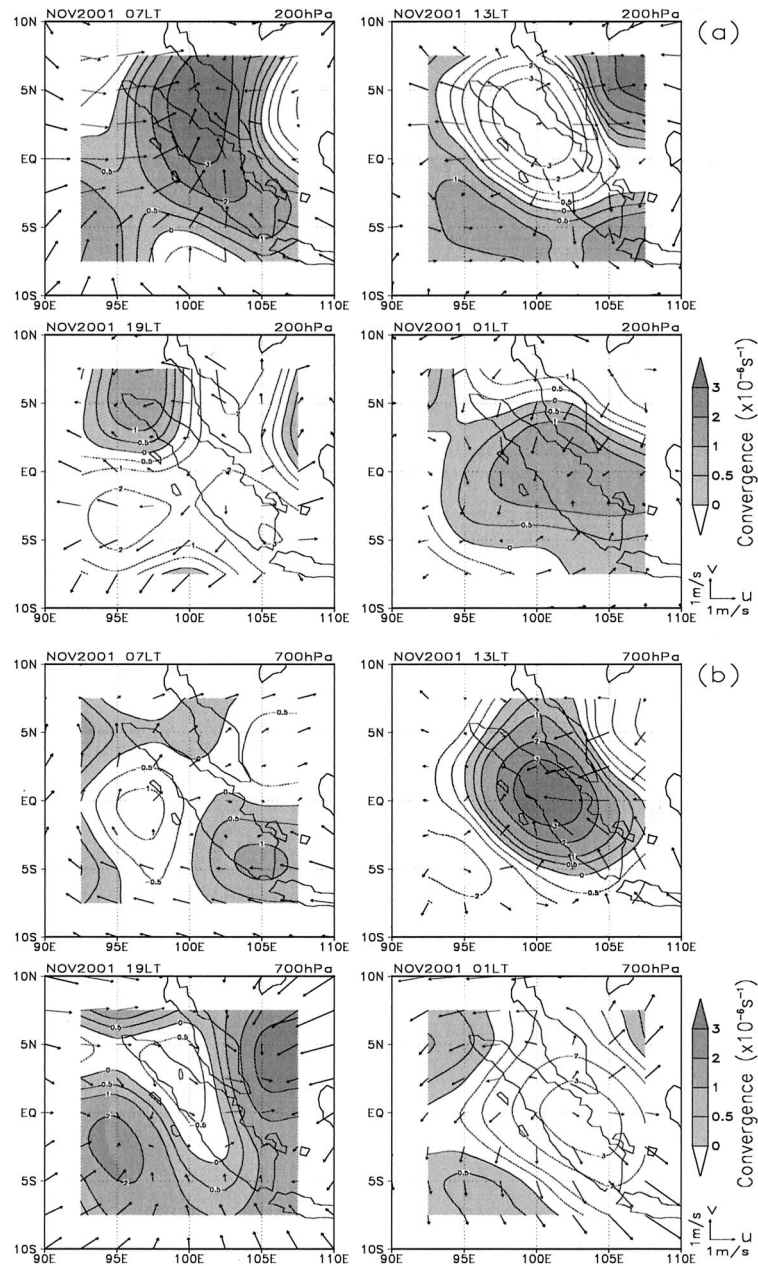


FIG. 11. Diurnal variations of horizontal wind anomaly (vectors) and convergence field (contours) at (a) 200 and (b) 700 hPa derived from the NCEP–NCAR reanalysis dataset averaged in Nov 2001. Each anomaly is calculated as a deviation from the monthly average value in this period.

vil) clouds. This feature is consistent with the result of Nesbitt and Zipser (2003), who showed that the rainfall maximum in the afternoon consists of small (non-MCS) features over land based on the TRMM 3-yr (1998–2000) database of precipitation features (PFs). After the total rainfall reaches its peak at 1700–1800 LT in the evening, the convective rainfall fraction decreases with time. In contrast, the convective rainfall fraction maintains approximately 50%–60% throughout the day over the coastal sea region. Especially, convective systems

composed of developed cumulonimbus with spread anvil are suggested to be a major portion of the precipitating clouds over the coastal sea region in the nighttime. However, because the peak times of convective and stratiform rainfalls are coincident over the coastal sea region in the early morning (around 0300–0600 LT) as shown in Figs. 5c and 5d, life cycles of convective cloud, eventually developing into an MCS, do not seem to be reasonable compared with those over the inland region in the late evening. Another possibility to be

mentioned in the next subsection is that stratiform rainfall over the coastal sea region comes from spread anvil clouds associated with developed cumulonimbus over the inland region conveyed by upper easterly winds. Nesbitt and Zipser (2003) showed that PFs with MCSs, developing mainly over the southwestern land region of Sumatera Island in the evening, started to expand their territory over the coastal sea region in the nighttime. This feature is also consistent with our results and supports the explanation of much stratiform rainfall fraction over the coastal sea region. Considering that the total rainfall amount over the southwestern coastal sea region is much greater than that over the land region as shown in Figs. 1a and 2, the latter process (advection of upper anvil clouds from the inland region) seems to be reasonable, and the anvil could have played the role of seeder cloud to the middle layer cloud beneath it. Similar kinds of heavy rainfall systems over the leeward side of the mountains, in which an upper-layer cloud (anvil) advected from the windward side of the mountain enhances the surface rainfall by seeding to the middle-layer cloud, have been studied (e.g., Iwanami et al. 1988; Takeda and Takase 1980). This may be one possible mechanism to explain why more rainfalls are shown over the farther offshore region ( $\sim 300$  km) in the early morning (Figs. 5a and 10).

Takayabu (2002) also distinguished convective and stratiform rainfalls in the diurnal variations using TRMM PR on both the land and the ocean over the entire globe. However, special attention has to be paid to the data over the ocean because rainfall characteristics are completely different between the coastal sea (including the offshore region in Fig. 1a) and isolated ocean regions, as shown in Figs. 1b and 5. The location of the boundary between these regions might be controlled by how far the rainfall peak migrates toward the offshore region. The distance of the rainfall peak migration for Sumatera Island is approximately 500 km off the southwestern coastline as shown in Fig. 5. Yang and Slingo (2001) showed phase propagation of the diurnal harmonic of cloud brightness temperature toward the offshore region in several areas, for example, the Bay of Bengal, southwestward away from the Mexican coast, and off the West African coast, as well as Indonesian islands including Sumatera. The rainfall peak of the Bay of Bengal extends its phase propagation up to 1000 km from the coastline with a propagation speed of  $15\text{--}20\text{ m s}^{-1}$ . Based on the results of previous sections, the characteristics of rainfall (e.g., convective rainfall fraction) over these regions are also thought to differ between the land and the offshore regions. Hence, it is appropriate to classify the globe into three regions of 1) land, 2) coastal sea region within 500–1000 km from the coastline, and 3) isolated ocean far from the coastline, similar to those definitions of Petersen and Rutledge (2001), when we examine the diurnal rainfall variation and its interaction with the large-scale atmosphere. Otherwise, the dataset may contain a bias due

to diurnal rainfall phase propagation (i.e., diurnal rainfall peak migration). This categorization seems to be particularly important when we study the water and energy circulations over the Indonesian Maritime Continent because it has huge areas of coastal sea and does not have the pure characteristics of either land or ocean for rainfall variations.

### b. Characteristics of rainfall peak migrations

Wind variations in the troposphere over both Kototabang and Tabing associated with the rainfall peak migration and their mechanism are examined in this subsection.

Based on the fact that the rainfall peak migrates from southwest to northeast in the daytime and the time of peak rainfall is 1600 LT over Kototabang, the variation of tropospheric wind at 2–3 km (easterly and northerly wind anomalies before rainfall peak passes through) in Fig. 9a suggests that circulation converging at the bottom of a convective cloud system located in the southwestern side of Kototabang is responsible for the rainfall peak. Westerly and southerly wind anomalies following the rainfall peak after 1600 LT are thought to be an airflow converging toward the convective system located in the northeastern side of Kototabang. On the other hand, the westerly wind anomaly at 2–3 km over Tabing in Fig. 9f increases from 1300 LT until its peak at 1900 LT. Then, it tends to decrease (becomes an easterly wind anomaly) during the time of heavy rainfall (2300–0100 LT) and reaches its minimum at 0100 LT. Based on the fact that the rainfall peak migrates from northeast to southwest in the nighttime and the rainfall peak time is at 2300–0100 LT over Tabing, the variation of tropospheric wind at 2–3 km (westerly wind anomaly before rainfall peak passes through) in Fig. 9f suggests that a circulation converging at the bottom of a convective cloud system located in the northeastern side of Tabing is responsible for the rainfall peak. The easterly wind anomaly following the rainfall peak is thought to be an airflow converging toward the convective system located on the southwestern side of Tabing.

Schematic pictures of diurnal land–sea rainfall peak migration and circulations related to the migration are shown in Fig. 12 based on the results mentioned above. Each picture shows a vertical cross section of the domain A–B as shown in Fig. 4a, but the horizontal scale is not the same as that in the figure. Based on the Figs. 6a and 7, westerly and easterly winds prevail over this area below and above 8 km, respectively. The former is indicated as “W” and the latter as “E” in this figure, and they are presumed to be large-scale background winds as shown in Figs. 6a and 7. First, we consider the rainfall peak migration toward the inland in the daytime. The shallow westerly wind, which is supposed to be a sea breeze (indicated by “S”), is observed at Tabing during 1000–1300 LT as shown in Fig. 8b. If an atmospheric instability is suitable, it is reasonable to con-

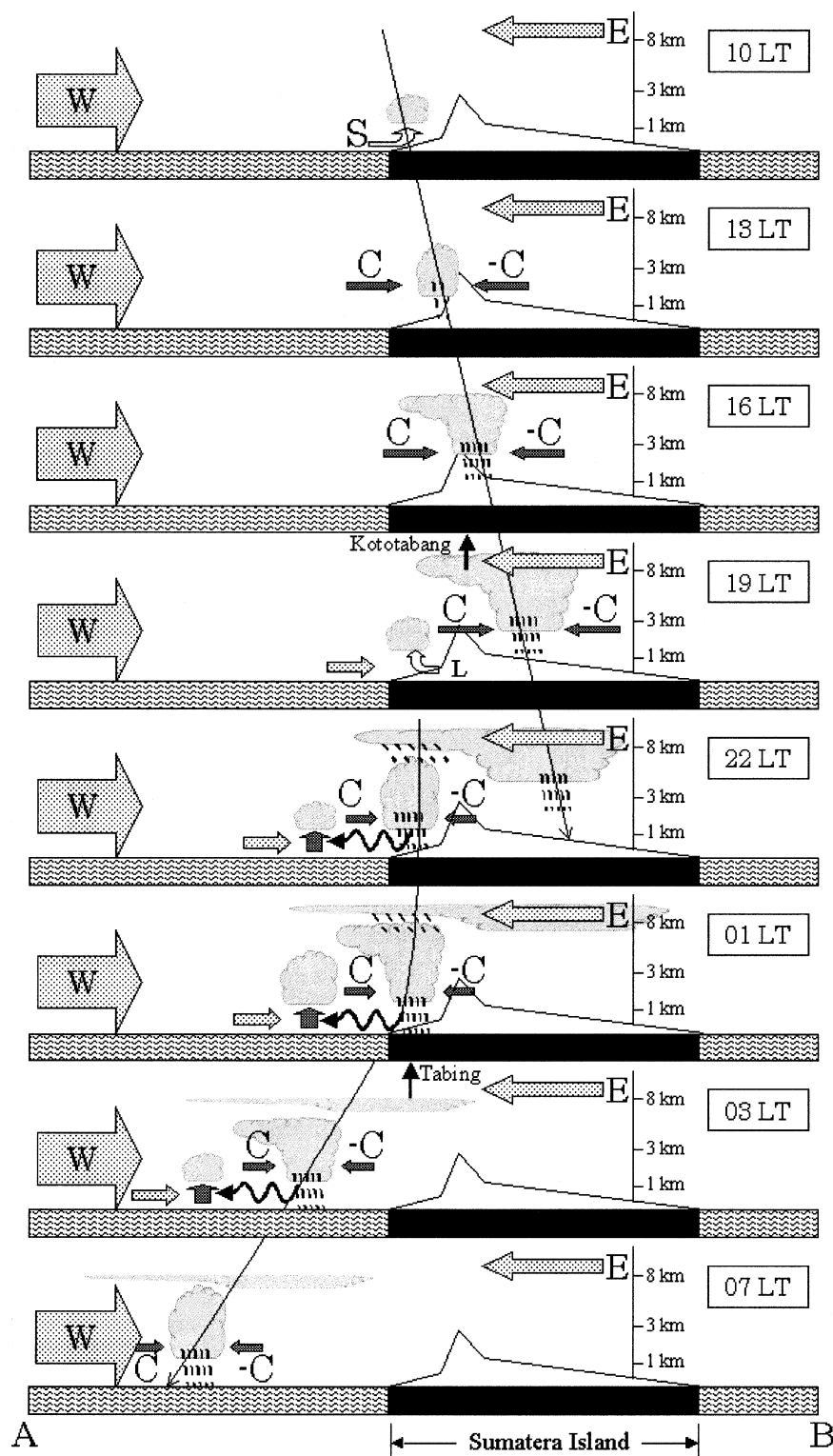


FIG. 12. Schematic pictures of diurnal land-sea rainfall peak migration and circulations related to the migration. Each picture shows a vertical cross section of the domain A-B as shown in Fig. 4a, but horizontal scale is not the same as in the figure. Each arrow indicates airflow related to the convection as follows: W: large-scale background wind predominant below 8 km; E: large-scale background wind predominant above 8 km; L: local land breeze flow below 1 km; S: local sea breeze flow below 1 km; C: converging airflow at the bottom of migrating convection that makes the local rainfall peak.

sider that the sea breeze acts as a trigger to generate an initial convection when the breeze meets the mountain range located along the southwestern coastline of Sumatera Island (just northeastern side of Taping station as shown in Fig. 4b). Indeed, developing clouds appeared first along the mountain range during 1000–1600 LT in Fig. 10. The developing convection, which is responsible for the local rainfall peak, migrates inland with time until the evening as shown in Fig. 5a. Based on the LCL analysis shown in Figs. 9d and 9i, the average height of the cloud base is presumed to be 1.0–1.5 km. The developed cloud-top height is roughly 220 K ( $T_{BB}$ ) as shown in Fig. 10, which corresponds to 12–13 km based on sounding data (not shown). Development of convection may be due to convergent flows as indicated by “C” and “-C” in Fig. 12 (southwesterly is positive). After the mature stage at 1900 LT, the developed convective cloud expands to form a stratiform anvil cloud area above 8 km in which the easterly wind is predominant as shown GMS IR1 images in Fig. 10. Local convergence between the background westerly wind and the land breeze (indicated as “W” and “L,” respectively, in Fig. 12) is presumed to appear at the southwestern foot of the mountains, which is shown after 0100 LT at Taping in Fig. 8b. Convection develops and generates rainfall there with converging airflows in the middle and lower levels (indicated by “C” and “-C” in Fig. 12) during 2200–0100 LT. Based on Fig. 5, we consider that the rainfall peak migrates to the offshore region until 0700 LT the next morning, against the background westerly wind in the lower troposphere.

If we consider the migration speed to be a constant  $10 \text{ m s}^{-1}$  from 1300 to 1900 LT, the convection can move 216 km ( $D$ ) from west to east over Kototabang. We also assume two-dimensional zonal airflow and no divergence in the meridional direction, and the convergence inside of the two-dimensional domain with the distance of  $D$  can be estimated by  $-(C_{13LT} - C_{19LT})/D$ , which equals approximately  $9.7 \times 10^{-6} \text{ s}^{-1}$ , where  $C_{13LT}$  and  $C_{19LT}$  mean local converging airflows over Kototabang at 1300 and 1900 LT, and they can be estimated from Fig. 9a as  $-1.1$  and  $1.0 \text{ m s}^{-1}$ , respectively. This convergence is one order of magnitude smaller than that of a mesoscale disturbance ( $\sim 10^{-5} \text{ s}^{-1}$ ) that causes heavy rainfall in middle latitudes, but it is considered a reasonable value because the calculation includes 4 days of no rainfall and is averaged over an area of approximately  $(300 \text{ km})^2$ . Furthermore, the order of the convergence is roughly consistent with that derived from the reanalysis dataset as shown in Fig. 11b. On the other hand, the lower-tropospheric convergence over the land in the afternoon as shown in Fig. 11b can be considered in two ways: (a) as a result of the heat contrast between the land and ocean, which will cause convection over the land as an average feature, and (b) as the average feature of cloud formation, as shown in Fig. 10, which causes the convergence over the land in the

afternoon. Apparently the reverse happens over the ocean in the late night.

Four main possible driving mechanisms have been proposed for the diurnal migration of convective systems: 1) an advection process due to large-scale background circulation, 2) an interaction between a gravity current (produced by cold downdrafts from the developed convective cloud) and an ambient wind near the surface, which makes a new convergence ahead of the old cloud system, 3) an upward current caused by gravity waves originating from the adjacent developed convective cloud system, and 4) thermal instability of the lower troposphere propagated by gravity waves originating in diurnally oscillating heat sources of the daytime mixed layer over the adjacent coastal land region. Satomura (2000) examined the diurnal phase delay of rainfall over the Indochina peninsula, observed by both GMS ( $T_{BB}$  and  $\Delta T_{BB}$ ) and a ground-based radar network, using a two-dimensional, nonhydrostatic, and cloud-resolving numerical model. The convective system generated on the leeside foot in the evening formed a squall line system and migrated eastward in the nighttime at  $5\text{--}10 \text{ m s}^{-1}$ . The results did not provide a clear mechanism of eastward migration but suggested that it might be a combination of both 1) and 2) because the convection formed a squall line system (i.e., a self-replicating mechanism of a mesoscale convective system) and it migrated faster than the low-level background westerly wind speed of  $6.5 \text{ m s}^{-1}$  at maximum. Shige and Satomura (2000) have also shown the importance of 3) in the development of a convective cell into a meso- $\beta$ -scale convective system over the tropical ocean and suggested that a new convection cell adjacent to the original cell was triggered by process 3) using a two-dimensional, nonhydrostatic, and cloud-resolving numerical model. On the other hand, Mapes et al. (2003a,b) and Warner et al. (2003) studied the westward migration of rainfall peaks to offshore regions at a speed of  $15\text{--}20 \text{ m s}^{-1}$ , against the background westerly wind in the lower troposphere, in the nighttime over northwestern South America. Based on the results of a three-dimensional, nonhydrostatic, and cloud-resolving numerical model, they concluded that 4) is a key mechanism of rainfall offshore migration in the nighttime.

Based on the observational results in the previous sections and the results of earlier studies, both advection by the background westerly wind in the lower troposphere and self-replicating mechanisms seem to be crucial causes of the inland migration in the daytime in the present study. It is easy to consider the background westerly wind as a primary driving force conveying the convective system eastward because the speed of rainfall peak migration is similar to that of zonal wind in the lower troposphere. However, our observations are not sufficiently detailed in space and time to support that possibility in this study. The self-replicating mechanism may also contribute to the migration because the migration speed of  $10 \text{ m s}^{-1}$  is faster than the maximum

background wind speed, which suggests that this mechanism plays an important role in the migration. In contrast to the daytime migration, both self-replicating and gravity wave mechanisms are thought to be essential for the rainfall peak migration toward the offshore region in the nighttime.

## 5. Concluding remarks

Regional variation of the diurnal rainfall cycle over Sumatera Island has been examined using TRMM PR, intensive rawinsonde soundings, GMS, OLR, surface observation, and objective reanalysis data, and the results are summarized as follows:

- 1) Approximately 70% of the rainfall over the inland region of Sumatera Island during the evening is convective. A sharp peak of convective rainfall in the evening is followed a few hours later by a weak peak of stratiform rainfall. In contrast, rainfall from midnight until early morning over the surrounding coastal sea region includes both convective and stratiform rain in almost equal measure. The amplitude of this diurnal variation decreases with distance from the coastline.
- 2) Regional variability of rainfall is caused by the migration of the rainfall peak from the coastline toward the inland region in the daytime and toward the offshore region in the nighttime. The distance of each rainfall peak migration from the coastline is up to 400 km, and the average speed of migration is approximately  $10 \text{ m s}^{-1}$ . The convective rainfall ratio over the land in the daytime reaches its maximum just before the time of rainfall peak and migrates inland with time. On the other hand, that over the ocean in the nighttime is almost unchanged with time and has no relation to the distance from the coastline.
- 3) Most convective clouds develop along the southwestern coastline of Sumatera Island (southwestern foot of the central mountains) between 1300 and 1600 LT. The obvious peak of developing cloud tops migrates toward the inland region from 1600 to 2200 LT, and its top height decreases gradually until 0100 LT. This life cycle of a cloud system is consistent with that of rainfall peak migration. On the other hand, high cloud top extends its area offshore to the coastal sea region during 2200–0400 LT. The rawinsonde sounding data both at Kototabang and Tabin show remarkable diurnal variations of winds at 2–3 km, formed by the convergence below the migrating convective system.
- 4) The following process is suggested regarding the rainfall peak migration based on the observational results. Initial convections in the late morning and in the late evening are generated along the southwestern foot of the mountains by local convergence of sea breeze against the mountains and land breeze against the background westerly wind. The former

migrates toward inland regions under the background westerly wind in the lower troposphere until the late evening accompanied with the local converging flow around the convection, and extended stratiform anvil clouds are advected westward by the easterly wind in the upper troposphere. The latter migrates toward the offshore region in the nighttime by generating new convection ahead of it (windward side) probably through the combination process of self-replicating and gravity wave mechanisms.

We have examined the diurnal land–sea rainfall peak migration as a large-scale average feature in this study, but the case study using 1-month and/or 1-week intensive sounding data do not represent a general climatological feature. Hence, it is important to proceed to highly detailed studies of individual cases more, employing not only the observation techniques used in this study but also both a ground-based radar system and a numerical model simulation as a next step. In addition, seasonal and intraseasonal differences of the migration features have to be examined in a future study.

**Acknowledgments.** The TRMM 3G68 dataset utilized in this study was published by TSDIS/NASA. GMS IR1 data were observed by Japan Meteorological Agency (JMA) and distributed by Kochi University, Japan. Rawinsonde observations were carried out based on a collaboration among the Agency for the Assessment and Application of Technology (BPPT) and the Indonesian Meteorological and Geophysical Agency (BMG) on the Indonesian side, and FORSGC, Kobe University, Kyoto University, and Hokkaido University on the Japanese side. The authors express their thanks to Drs. Masaki Katsumata, Taro Shinoda, and Hisayuki Kubota for their helpful discussions and positive comments. Thanks are also extended to the constructive comments of two anonymous reviewers who greatly improved the content of this manuscript. A part of this study was financially supported by the Grant-in-Aid for Scientific Research (C) 14595007 (representative: Shuichi Mori) of the Japan Society for the Promotion of Science (JSPS).

## REFERENCES

- Asai, T., S. Ke, and Y. Kodama, 1998: Diurnal variability of cloudiness over East Asia and the western Pacific Ocean as revealed by GMS during the warm season. *J. Meteor. Soc. Japan*, **76**, 675–684.
- Awaka, J., T. Iguchi, and K. Okamoto, 1998: Early results on rain type classification by the Tropical Rainfall Measuring Mission (TRMM) precipitation radar. *Proc. Eighth URSI Commission F Open Symp.*, Aveiro, Portugal, URSI, 143–146.
- Gray, W. M., and R. W. Jacobson Jr., 1977: Diurnal variation of deep cumulus convection. *Mon. Wea. Rev.*, **105**, 1171–1188.
- Grody, N. C., 1984: Precipitation monitoring over land from satellites by microwave radiometry. *Proc. IGARSS '84 Symp.*, Strasbourg, France, IEEE, 417–422.
- Hamada, J.-I., M. D. Yamanaka, J. Matsumoto, S. Fukao, P. A. Winarso, and T. Sribimawati, 2002: Spatial and temporal variations

- of the rainy season over Indonesia and their link to ENSO. *J. Meteor. Soc. Japan*, **80**, 285–310.
- Harada, S., T. Oki, and K. Musiake, 1998: Diurnal variation and its seasonal variation of convective activity over the Indochina Peninsula region by GMS-IR data (in Japanese with English abstract). *J. Japan Soc. Hydrol. Water Resour.*, **11**, 371–381.
- Heymsfield, G. M., and R. Fulton, 1992: Modulation of SSM/I microwave soil radiances by rainfall. *Remote Sens. Environ.*, **39**, 187–202.
- Houze, R. A., Jr., 1977: Structure and dynamics of a tropical squall line system. *Mon. Wea. Rev.*, **105**, 1540–1567.
- , 1982: Cloud clusters and large-scale vertical motions in the Tropics. *J. Meteor. Soc. Japan*, **60**, 396–410.
- , and A. K. Betts, 1981: Convection in GATE. *Rev. Geophys. Space Phys.*, **19**, 541–576.
- , S. G. Geotis, F. D. Marks Jr., and A. K. West, 1981: Winter monsoon convection in the vicinity of north Borneo. Part I: Structure and time variation of the clouds and precipitation. *Mon. Wea. Rev.*, **109**, 1595–1614.
- Iwanami, K., K. Kikuchi, and T. Taniguchi, 1988: A possible rainfall mechanism in the Orofune mountain range, Hokkaido, Japan—The rainfall enhancement by a two-layer cloud structure. *J. Meteor. Soc. Japan*, **66**, 497–504.
- Janowiak, J. E., P. A. Arkin, and M. Morrissey, 1994: An examination of the diurnal cycle in oceanic tropical rainfall using satellite and in situ data. *Mon. Wea. Rev.*, **122**, 2296–2311.
- Johnson, R. H., and D. C. Kriete, 1982: Thermodynamic and circulation characteristics of winter monsoon tropical mesoscale convection. *Mon. Wea. Rev.*, **110**, 1898–1911.
- Kalnay, E., and Coauthors, 1996: The NCEP/NCAR 40-Year Reanalysis Project. *Bull. Amer. Meteor. Soc.*, **77**, 437–471.
- Kistler, R., and Coauthors, 2001: The NCEP–NCAR 50-year reanalysis: Monthly means CD-ROM and documentation. *Bull. Amer. Meteor. Soc.*, **82**, 247–267.
- Kubota, H., and T. Nitta, 2001: Diurnal variations of tropical convection observed during the TOGA-COARE. *J. Meteor. Soc. Japan*, **79**, 815–830.
- Mapes, B. E., T. T. Warner, and M. Xu, 2003a: Diurnal patterns of rainfall in northwestern South America. Part III: Diurnal gravity waves and nocturnal convection offshore. *Mon. Wea. Rev.*, **131**, 830–844.
- , —, —, and A. J. Negri, 2003b: Diurnal patterns of rainfall in northwestern South America. Part I: Observations and context. *Mon. Wea. Rev.*, **131**, 799–812.
- Mohr, K. I., J. S. Famiglietti, and E. J. Zipser, 1999: The contribution to tropical rainfall with respect to convective system type, size, and intensity estimated from the 85-GHz ice-scattering signature. *J. Appl. Meteor.*, **38**, 596–606.
- Murakami, M., 1983: Analysis of the deep convective activity over the western Pacific and southwest Asia. Part I: Diurnal variation. *J. Meteor. Soc. Japan*, **61**, 60–76.
- Murata, F., and Coauthors, 2002: Relationship between wind and precipitation observed with a UHF radar, GPS rawinsondes, and surface meteorological instruments at Kototabang, west Sumatra during September–October 1998. *J. Meteor. Soc. Japan*, **80**, 347–360.
- Neale, R., and J. Slingo, 2003: The Maritime Continent and its role in the global climate: A GCM study. *J. Climate*, **16**, 834–848.
- Negri, A. J., T. L. Bell, and L. Xu, 2002: Sampling of the diurnal cycle of precipitation using TRMM. *J. Atmos. Oceanic Technol.*, **19**, 1333–1344.
- Nesbitt, S. W., and E. J. Zipser, 2003: The diurnal cycle of rainfall and convective intensity according to three years of TRMM measurements. *J. Climate*, **16**, 1456–1475.
- Nitta, T., and S. Sekine, 1994: Diurnal variation of convective activity over the tropical western Pacific. *J. Meteor. Soc. Japan*, **72**, 627–641.
- Ohsawa, T., H. Ueda, T. Hayashi, A. Watanabe, and J. Matsumoto, 2001: Diurnal variations of convective activity and rainfall in tropical Asia. *J. Meteor. Soc. Japan*, **79**, 333–352.
- Okamoto, N., M. D. Yamanaka, S.-Y. Ogino, H. Hashiguchi, N. Nishi, T. Sribimawati, and A. Numaguti, 2003: Seasonal variations of tropospheric wind over Indonesia: Comparison between collected operational rawinsonde data and NCEP reanalysis for 1992–99. *J. Meteor. Soc. Japan*, **81**, 829–850.
- Oki, T., and K. Musiake, 1994: Seasonal change of the diurnal cycle of precipitation over Japan and Malaysia. *J. Appl. Meteor.*, **33**, 1445–1463.
- Okumura, K., T. Satomura, and W. Khantiyanan, 2003: Diurnal variation of precipitation by moving mesoscale systems: Radar observations in northern Thailand. *Geophys. Res. Lett.*, **30**, 2073, doi:10.1029/2003GL018302.
- Petersen, W. A., and S. A. Rutledge, 2001: Regional variability in tropical convection: Observations from TRMM. *J. Climate*, **14**, 3566–3586.
- , —, and R. E. Orville, 1996: Cloud-to-ground lightning observations from TOGA COARE: Selected results and lightning location algorithms. *Mon. Wea. Rev.*, **124**, 602–620.
- Ramage, C. S., 1968: Role of a tropical “maritime continent” in the atmospheric circulation. *Mon. Wea. Rev.*, **96**, 365–370.
- Renggono, F., and Coauthors, 2001: Precipitating clouds observed by 1.3-GHz boundary layer radars in equatorial Indonesia. *Ann. Geophys.*, **19**, 889–897.
- Rickenbach, T. M., and S. A. Rutledge, 1998: Convection in TOGA COARE: Horizontal scale, morphology, and rainfall production. *J. Atmos. Sci.*, **55**, 2715–2729.
- Rodgers, E., and H. Siddalingaiah, 1983: The utilization of Nimbus-7 SMMR measurements to delineate rainfall over land. *J. Climate Appl. Meteor.*, **22**, 1753–1763.
- Satomura, T., 2000: Diurnal variation of precipitation over the Indo-China Peninsula: Two-dimensional numerical simulation. *J. Meteor. Soc. Japan*, **78**, 461–475.
- Shige, S., and T. Satomura, 2000: The gravity wave response in the troposphere around deep convection. *J. Meteor. Soc. Japan*, **78**, 789–801.
- Sorooshian, S., X. Gao, K. Hsu, R. A. Maddox, Y. Hong, H. V. Gupta, and B. Imam, 2002: Diurnal variability of tropical rainfall retrieved from combined GOES and TRMM satellite information. *J. Climate*, **15**, 983–1001.
- Steiner, M., R. A. Houze Jr., and S. E. Yuter, 1995: Climatological characterization of three-dimensional storm structure from operational radar and rain gauge data. *J. Appl. Meteor.*, **34**, 1978–2007.
- Takayabu, Y. N., 2002: Spectral representation of rain profiles and diurnal variations observed with TRMM PR over the equatorial area. *Geophys. Res. Lett.*, **29**, 1584, doi:10.1029/2001GL014113.
- Takeda, T., and K. Takase, 1980: Radar observation of rainfall system modified by orographic effects. *J. Meteor. Soc. Japan*, **58**, 500–516.
- Warner, T. T., B. E. Mapes, and M. Xu, 2003: Diurnal patterns of rainfall in northwestern South America. Part II: Model simulations. *Mon. Wea. Rev.*, **131**, 813–829.
- Williams, C. R., W. L. Ecklund, and K. S. Gage, 1995: Classification of precipitating clouds in the Tropics using 915-MHz wind profilers. *J. Atmos. Oceanic Technol.*, **12**, 996–1012.
- Wu, P., J.-I. Hamada, S. Mori, Y. I. Tauhid, M. D. Yamanaka, and F. Kimura, 2003: Diurnal variation of precipitable water over a mountainous area of Sumatra Island. *J. Appl. Meteor.*, **42**, 1107–1115.
- Yang, G.-Y., and J. Slingo, 2001: The diurnal cycle in the Tropics. *Mon. Wea. Rev.*, **129**, 784–801.